Turkish Journal of Remote Sensing and GIS
Türk Uzaktan Algılama ve CBS Dergisi

Turk J Remote Sens GIS, March 2023, 4(1): 100-113
Journal homepage: http://www.dergipark.org.tr/en/pub/rsgis

Flood Inundation Mapping with Supervised Classifiers: 2021 Gediz Plain Flood

Denetimli Sınıflandırıcılarla Taşkın Haritalaması: 2021 Gediz Ovası Seli

Enis Arslan[1*], Serkan Kartal[2]

[1]*Çanakkale Onsekiz Mart University, Department of Computer Engineering, 17020, Çanakkale/Türkiye.*
[2]*Çukurova University, Department of Computer Engineering, 01380, Adana/Türkiye.*

ORIGINAL PAPER

***Corresponding author:**
Enis Arslan
enisarslan@gmail.com

doi: 10.48123/rsgis.1220879

Article history
Received: 18.12.2022
Accepted: 15.03.2023
Published: 28.03.2023

Abstract

Generation of flood inundation maps is beneficial in flood risk assessment and evaluation. Flood inundation mapping can be achieved by many remote sensing techniques like change detection (CD) with thresholding and machine learning-based (ML) methods. Optical and synthetic aperture radar (SAR) imagery are widely used, provided by different satellite systems. This study used Sentinel-1 SAR and Sentinel-2 MSI satellite data in Google Earth Engine (GEE) with supervised ML algorithms. Gediz Plain, Turkey was selected as the study area, which is an agricultural area covered mostly by croplands. A flood event that occurred on February 2, 2021, was examined and flood inundation map for the study area was composed. Support Vector Machines (SVM), Random Forest (RF) and K-Nearest Neighbor (KNN) ML algorithms were selected and models were trained with manually created labelled data in GEE. Also, CD was applied on after and before event SAR images in a traditional approach. RF classifier performs best in Sentinel-2 MSI imagery with 94% overall classification accuracy where KNN classifier gives 93.3% accuracy value for Sentinel-1 SAR dataset, indicating the robustness of SAR imagery for all-weather conditions.

Keywords: *Flood mapping, GEE, Classifier, Sentinel-1, Sentinel-2*

Özet

Taşkın haritalarının oluşturulması, taşkın sebepli risklerin değerlendirilmesinde oldukça faydalıdır. Sel-taşkın haritalaması, eşikleme ile değişiklik tespiti (DT) ve makine öğrenimi tabanlı (MÖ) yöntemler gibi birçok uzaktan algılama tekniği ile gerçekleştirilebilmektedir. Bu çalışmalarda farklı uydu sistemleri tarafından sağlanan optik ve sentetik açıklıklı radar (SAR) görüntüleri yaygın olarak kullanılmaktadır. Bu çalışmada, denetimli MÖ algoritmaları ile Google Earth Engine'de (GEE) Sentinel-1 SAR ve Sentinel-2 MSI uydu verileri kullanılmıştır. Çalışma alanı olarak Türkiye'nin Gediz Ovası seçilmiştir ve bu alan çoğunlukla ekili arazilerle kaplıdır. Bu çalışmada 2021 yılı Şubat ayının ikinci günü meydana gelen taşkın olayı incelenmiş ve çalışma alanı için taşkın haritası oluşturulmuştur. Çalışma için, Support Vector Machines (SVM), Random Forest (RF) ve K-nearest Neighbor (KNN) MÖ algoritmaları seçilmiş ve modeller GEE'de manuel olarak oluşturulan etiketlenmiş verilerle eğitilmiştir. Ayrıca geleneksel yaklaşımla olay öncesi ve sonrası SAR görüntülerine DT uygulanmıştır. RF sınıflandırıcısı, %94 genel sınıflandırma doğruluğu ile Sentinel-2 MSI görüntülerinde en iyi performansı gösterirken, KNN sınıflandırıcı, Sentinel-1 SAR veri kümesi için %93,3 doğruluk değeri vererek SAR görüntülerinin tüm hava koşulları için uygunluğunu göstermektedir.

Anahtar kelimeler: *Taşkın haritalaması, GEE, Sınıflandırıcı, Sentinel-1, Sentinel-2*

1. Introduction

Floods are natural disasters that occur as inundations after intense rainfall. They may cause loss of life, property damage, and communication line and transportation system failures in urban areas. It is the deadliest kind of disaster with a 43.5% death ratio (Chen et al. 2021). In remote sensing, satellite data with various spatial and temporal resolutions are widely used in a cost-effective way to determine the extent of flooding over large regions. Satellite imagery are introduced in two types: optical and synthetic aperture radars (SAR). Landsat and Sentinel-2 missions present optical imagery from visible bands to shortwave infrared (SWIR). On the other hand, Sentinel-1 mission provide SAR imagery with two polar-orbiting satellites, free of charge (Clement et al. 2018).

Nowadays, Satellite-borne SARs are used in a large extent for earth observation due to their near real-time all-weather and all-time capabilities. SAR systems emit radar signals to penetrate obstacles like clouds (Solbø and Solheim, 2005). SAR systems basically operate on backscatter radio signals reflecting from the surface of terrains like land or water and acquired by a satellite sensor. Radio signal strength depends on the roughness of the surface and rough surfaces like water are seen as dark in the images. Also, there are some drawbacks of SAR images where returning of the radio signal depends on some parameters like rain and winds that may cause waves on the water terrain (Čotar et al. 2016). Many satellite systems provide SAR images for use such as Sentinel-1, RADARSAT-1/2, TerraSAR-X and ENVISAT ASAR. Sentinel-1A and Sentinel-1B satellites can provide images with a frequency of 6 days but when they operate together with two orbits, they can observe any point of the earth in every six days.

SAR images can be used in various applications like flood extent mapping (Cao et al. 2019), water surface detection (Martinis et al. 2015), flood depth estimation (Cian et al. 2018), flooded vegetation detection (Klemas, 2013), flood risk assessment (Pramanick et al. 2022), oil spill detection (Topouzelis, 2008) and ship detection (Chang et al. 2019). When SAR-based flood extent mapping is the case, many methods and their combinations are used by the researchers. These are, texture analysis (Pradhan et al. 2014), region growing (Baghi and Karami, 2017), supervised classification (Benoudjit and Guida, 2019), unsupervised classification (Carincotte et al. 2006) and histogram thresholding (Brown et al. 2016). Texture analysis is a technique that examines and calculates textures in an image by using the first order and second order statistics. The region growing method calculates similarities between neighboring pixels and creates uniform regions while detecting edges. Supervised classification methods require training images labelled as flooded/non-flooded. Training images can be any image of the event including flooded and non-flooded areas. These areas can be manually labelled before training. Also, there are some techniques used to prepare training images automatically by applying a log ratio to an image captured before and after the flood event. Following the preparation of the dataset, any supervised classifier can be used for the classification of the land cover. Contrary to supervised methods, no labelled datasets are required for unsupervised classification methods. Unsupervised methods are mostly used for change detection in order to compose difference images. Change detection process provides a difference image by comparing the flooding time image with a previous dry scene of the study area. Generally, a threshold is applied to the difference images to classify the flooded areas. Among all these methods, histogram thresholding is the most common technique used for flood detection, which basically measures the backscatter signal from the terrain. Initially, a threshold is determined by examining the histogram of the event image, and selected threshold is applied to the image to classify it as flooded and non-flooded. This threshold can be defined manually by visual observation or automatically, by using Schumann's (Schumann et al. 2010) method, which calculates a global threshold value from the histogram by using Otsu's method (Kurita et al. 1992).

The objective of this study is to extract the inundation map of a flood event on February 2, 2021, in the Gediz plain, located in the western region of Turkey, by using remote sensing data and techniques. The Gediz plain is frequently subject to floods. Local news media agencies give information about the floods on two different days in February 2021. According to one news, the first heavy rainfall in the region was on 02.02.2021. Other news dated 14.02.2021 claims rainfall during a week. This region is economically important with fertile croplands, mostly as vineyards. In 1951, Turkish ministry council has decided a reserve area of 400 m around the Gediz river as a precaution to flood events. Flood mapping studies for this region can help officials to take necessary measures in advance. In this study, non-parametric supervised classifiers Random Forest (RF) (Breiman, 2001), Support Vector Machines (SVM) (Hsu et al. 2016), and K-Nearest Neighbor (KNN) (Duda et al. 1973) with optical and synthetic aperture radar (SAR) imagery were used to examine the flood extent. Performances of these classifiers were also evaluated on the study area. In a recent study (Ozkan and Tarhan, 2016), a flood risk assessment of the Gediz, Bakırçay, and Menderes regions was presented. Our study differentiates from this study by specifically focusing on flood mapping on a specific event using remote sensing techniques. To our knowledge, no study has been performed with remote sensing techniques with supervised classifiers in our study area.

2. Study Area

The study area was selected as Gediz River Delta which is located in the Aegean region, in the western part of Turkey. Gediz Delta (38°300 N, 26°550 E), covering nearly an area of 400 km^2, is an ecosystem formed by aluvions drained by Gediz River. Gediz River starting from Kütahya (Murat and Şaphane mountains) to Uşak and Manisa provinces ends in İzmir province, which is the major province of the region with nearly 4.3 million habitants. Gediz Delta is known with its fertile agricultural lands. Menemen plain, a part of the region, supplies nearly 40% of the spinach production of Turkey. Also cotton, fruit and legumes are the main farming items in the region (ÇOB, 2007). Gediz Delta, with a biogeographic diversity host nearly 80,000 wetland birds in a year (Arslan et al. 2021). The study area is given in Figure 1.

Figure 1. Study area

Study area, mainly located in Manisa province, with a Mediterranean climate, hot dry summer and mild winter conditions. Mean annual rainfall of 724 mm, mostly in winter, 123 mm in January. Long-term mean annual temperature is 17°C, with minimum and maximum values of 3°C and 10°C in January, respectively. Highest daily rainfall was recorded on 12.23.1986 with the value 163,5 mm (MGM, 2023).

Gediz Delta was selected for investigation because of the recurrent flooding events on the fertile agricultural fields. According to news media in April, 2012, heavy rainfall over levelled the Demirköprü Dam and officials released the extent water out of the Dam in a controlled way. But this caused 30 thousand m^2 area to inundate and crops were damaged.

3. Data and Methods

In this study Sentinel-1 SAR and Sentinel-2 MSI data products are used for flood inundation mapping of the Gediz plain. For the flood event, Sentinel-2 MSI data was used for validation by using spectral indices due to the absence of ground truth.

Actually, in this study, Sentinel-2 MSI data provided little help in the validation process because of the high cloudiness level on the event day and following days. A special SWIR composite obtained from Sentinel-2 MSI satellite with bands B12, B2 and B3, apparently showed the flooded areas, with acceptable cloud disturbances. Also, this composite was useful for defining polygons to be used for training and validation purposes. Google Earth Engine (GEE) (Gorelick et al. 2017) is a cloud platform provided by Google Inc. GEE provides high-computing power with an extensive set of satellite data and several machine learning (ML) algorithms. GEE platform was used for data access, computing, and visualization.

3.1 Data

In the scope of this study, images of Sentinel-1 SAR and Sentinel-2 MSI satellite systems introduced by European Space Agency (ESA) were used. A huge amount of satellite data is now available and reachable from GEE without charge. Sentinel-1 SAR data (VV and VH polarizations) was used for the initial observation of the flood inundation. On the event date (02-02-2021) Sentinel-1 SAR image was available while Sentinel-2 MSI image was not available for the event date. The earliest optical image was on 06-02-2021 with 10.28% cloudy pixel average. The satellite data used is given in Table 1.

Table 1. Satellite data obtained and used in GEE as before/after a flood event

Dataset	Before event dates	After event dates	Spatial Resolution (m)
Sentinel-1 SAR GRD:C Band (VV-VH)	2020-12-23	2021-02-03	10 m for VV and VH polarizations
Sentinel-2 MSI Level 2-A	2021-01-17 2021-01-19	2021-02-06	10 m for bands 'B2', 'B3', 'B4', 'B8', 20 m for bands 'B11', 'B12'

3.1.1 Selection of Training and Validation Data

Using supervised classification algorithms in GEE requires labelled data. A collection of accurate training samples is required to avoid uncertain classification results. For this purpose, training data and validation data were prepared by manual interpretation of the study area as polygons by using the GEE interface. Extreme care was taken to select polygons as homogenous as possible. Polygon counts are given in Table 2 where *S2* and *S1* acronyms denote Sentinel-2 and Sentinel-1 satellites, respectively.

Table 2. Polygon statistics which represent class labels as feature collections

S2	**water**	**non-vegetated**	**vegetated**	**forest**	**cloud**
Train	30	30	30	30	10
Validate	30	30	30	30	10
S1	**water**	**other areas**			
Train	20	20			
Validate	20	20			

In Table 2, land cover class labels for Sentinel-2 imagery (SWIR composite) were defined as: water, non-vegetated, vegetated, forest, and cloud. Cloud was added as a feature in order to visualize the final classification map easily. On the other hand, another set of polygons were created for Sentinel-1 SAR imagery classification as water and other areas. Distinct polygons were selected for training and validation processes. For each class, polygons are obtained by polygon tool on GEE.

Different approaches were tried to compose accurate polygons. Spectral indices were insufficient to demonstrate the flooded areas because of the cloud effect. Therefore, a SWIR composite (bands B12, B2 and B3), given in Figure 2, was used to label areas covered with water for water class. Other class labels were selected from the most evident spectral indices image (NDWI).

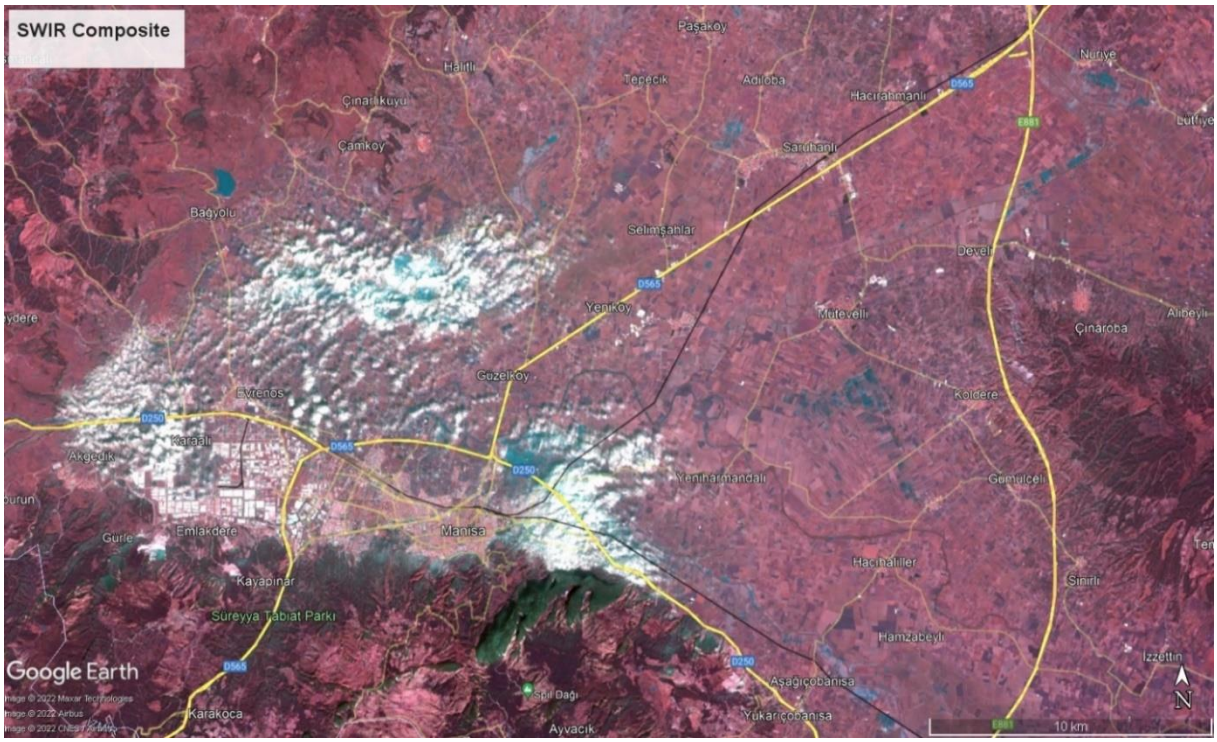

Figure 2. SWIR composite (RGB: B12, B2, B3) of the study area

In Figure 2, flooded areas can be seen in blue color mostly surrounded by clouds. This image composite was the most obvious one for the flood event when compared to others. For the SAR classification, Sentinel-1 SAR after event image (VH) was used to determine the polygons.

3.2 Methods

This study is composed of two stages. In the first stage, generic SAR preprocessing and change analysis methodology were applied to find out the inundated areas. In the second stage, supervised classification was applied to optical and SAR images, distinctly. The whole methodology workflow of the study is given in Figure 3.

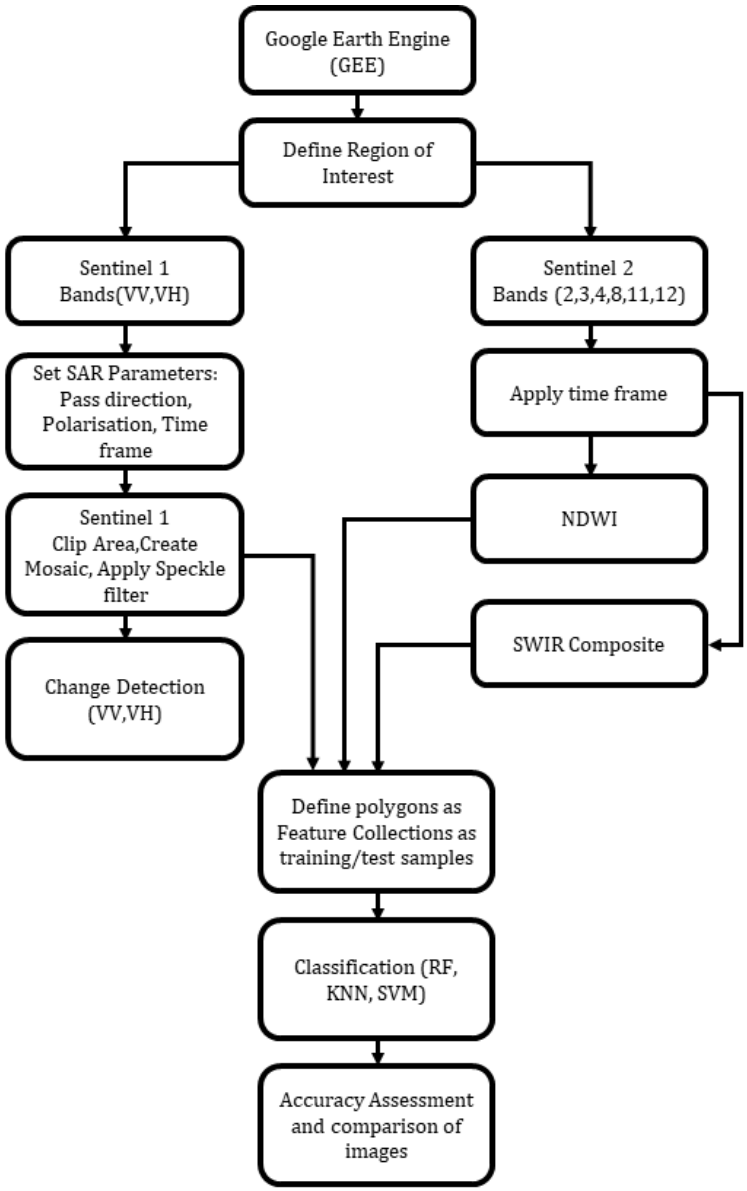

Figure 3. Methodology workflow of the study

Satellite data was filtered with region of interest (ROI) i.e. study area, bands needed (VV and VH), event dates, and pass direction (DESC) for Sentinel-1. The resulting image was clipped and mosaicked. A speckle filter with a radius of 100m was applied for smoothing. On the other hand, for Sentinel-2 Optical images, a cloud filter and time frame filter were applied for the nearest event dates using the same ROI. Normalized Difference Vegetation Index (NDVI) (Rouse et al. 1974), Normalized Difference Water Index (NDWI) (McFeeters, 1996) Normalized Difference Moisture Index (NDMI) (Hardisky et al. 1983), and Modified NDWI (MNDWI) (Xu, 2006) spectral indices were calculated for the resulting Sentinel-2 collections. Spectral indices were not successful in visualizing flooded areas because of the cloudiness of the optical image. NDWI was slightly better when compared to others, and this image was selected for the classification of the study area The SWIR composite was composed to observe floodwater and used for creation of polygons as features (Figure 3).

3.2.1 SAR Change Detection

Sentinel-1 SAR data was used to expose inundated areas with a change detection method. Although there are several methods for change detection like post classification comparison as an unsupervised method, image differencing, image rationing and Principal component analysis (PCA). In this study, change detection was applied with image differencing technique.

This technique operates as subtracting pixel values (as digital numbers) for each corresponding bands and application of a threshold value to each band image to delineate the resulting change images. Generally, change images are compared to reference images, if they exist, resulting in an error matrix (Afify, 2011).

3.2.2 Classification Algorithms

In this study, Random Forest (RF) (Breiman, 2001), Support Vector Machines (SVM) (Hsu et al. 2016), and K-Nearest Neighbor (KNN) (Duda et al. 1973) machine learning (ML) algorithms were used for the classification of optical and SAR images. These classifiers are able to classify the input data by learning from the training data. Default parameters were used for all three algorithms. Only for RF, number of trees parameter was set to 10. Comparison table for these classifiers are given in Table 3.

Table 3. SVM, RF and KNN classifiers advantages/disadvantages (Thanh Noi and Kappas, 2017)

Classifier	Advantage	Disadvantage
Support Vector Machine (SVM)	Insensitive to noise/overtraining	Less sensitive to training dataset size
Random Forest (RF)	Robust to noise in data. Insensitive to noise/overtraining	Size and imbalanced data of training samples has more impact on the classification accuracy
k-Nearest Neighbor (KNN) classifier	Adjusts to multi class problems without any extra efforts.	Ideal value for the k parameter is hard to set, if k is too small it may lead to overfitting

Random Forest (RF)

RF algorithm is widely used in remote sensing applications. It is stable and efficient in runtime. RF combines many decision trees which are built during the training process. Training samples and variables are randomly selected. Each training sample is assigned to a class by using majority voting within these trees. The performance of the classifier is evaluated with samples not used in the training process. For each node, a random feature is selected from the feature set to split the tree properly. Generally, two parameters are used in RF: the number of trees and the number of nodes (Taheri Dehkordi et al. 2022; Amani et al. 2019).

Support Vector Machines (SVM)

SVM is a supervised ML method which is commonly used for regression and classification purposes. It is advantageous to use it when the sample size is small and in high dimensional feature space. SVM aims to find the optimal hyperplanes by using the training data to separate classes. Extreme vectors i.e. support vectors are selected to generate the hyperplanes. Kernel function type, gamma value, and cost value are the parameters of this algorithm. The linear kernel is used to project the input space to higher spaces when the data volume is high in order to separate the data (Taheri Dehkordi et al. 2022; Amani et al. 2019).

K-nearest Neighbor (KNN)

KNN is a non-parametric ML method that is commonly used for statistical applications. The algorithm finds the K-nearest samples to unknown samples by using the distance functions. The K value is the single parameter that can be defined by using bootstrap techniques (Thanh Noi and Kappas, 2017).

3.2.3 Accuracy Calculation

An error matrix is commonly used to calculate the accuracy of a classification. The degree of closeness of classification results to the values accepted as true is measured with accuracy term. Error matrix is used to determine overall accuracy consumer accuracy, producer accuracy and kappa statistics (Damtea et al. 2020). Overall Accuracy (OA) metric is in this study, classification accuracy has been calculated as the overall accuracy (OA) after validation and kappa coefficient (κ) (Cohen, 1960) was calculated by using the error matrix output of GEE for each classifier.

Kappa coefficient is a statistical measure which evaluates the agreement between training and validation. (κ) takes values in range (–1,+1) and values greater than 0.5 implies that it is in good agreement with classification (Taati et al. 2015).

3.2.4 Spectral Index Analysis

Optical images which are nearest to the event day (as given in Table 1) were mostly covered with clouds. These image composites are given in Figure 4.

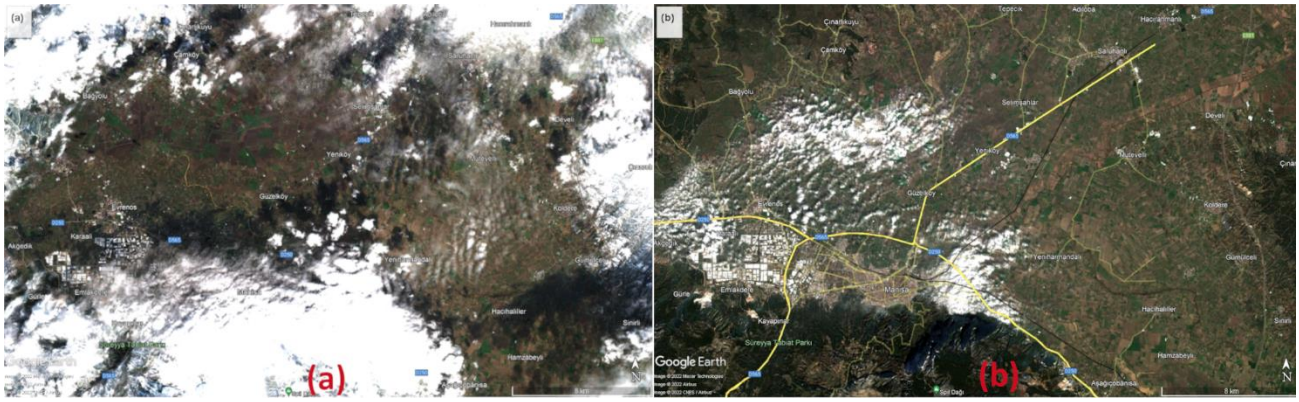

Figure 4. a) Sentinel-2 MSI before event image composite, b) Sentinel-2 MSI after event image

As seen in Figure 4, the image composite representing 'before event' dates have a high rate of cloud (left). The right image composite has a lower cloud rate but when Sentinel-1 SAR images have been examined it was seen that the cloudy area covers most of the flooded area. Because of that, change detection for optical images would not provide accurate evidences of flood. Spectral indice usage is an alternative to discriminate areas covered with water in an unsupervised manner. In order to discover flooded areas with spectral indices, NDVI (Normalized Difference Vegetation Index), NDWI (Normalized Difference Water Index), mNDWI (modified NDWI) and NDMI (Normalized Difference Moisture Index) were applied to Sentinel-2 MSI after event image. Formulas are given in Table 4.

Table 4. The spectral indices (Goffi et al. 2020)

Index	Formula	Reference
NDVI	(NIR – RED) / (NIR + RED)	Rouse et al. 1974
MNDWI	(GREEN – SWIR1) / (GREEN + SWIR1)	Xu, 2006
NDWI	(GREEN – NIR) / (GREEN + NIR)	McFeeters, 1996
NDMI	(NIR – SWIR) / (NIR + SWIR)	Hardisky, 1983

None of the images composed by spectral indices given in Table 4 was helpful to discriminate land covered with water, even special indices for water identification (NDWI, MDNWI). This is mostly because of the cloud overage in flooded areas. Output images of spectral indices are given in Figure 5.

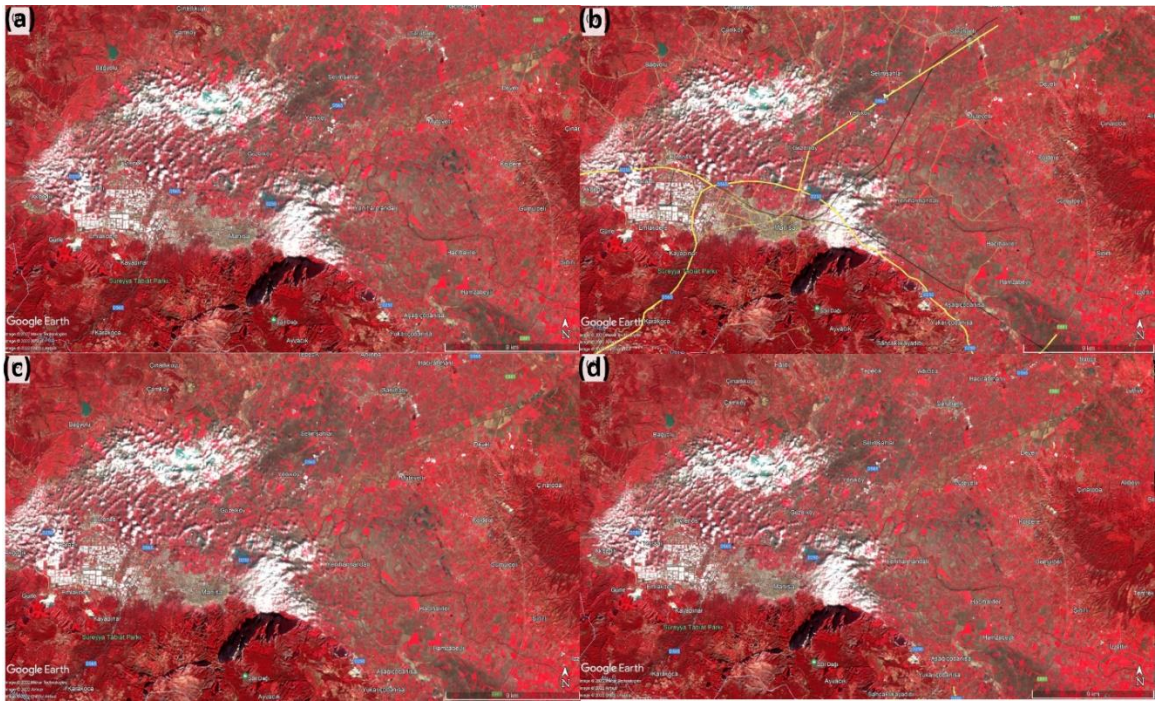

Figure 5. a) Output images of spectral indices MNDWI, b) NDMI, c) NDVI and d) NDWI

As seen in Figure 5, four of the spectral indices of Sentinel-2 MSI image on 2021-02-06 provide very similar results. After visual checking of these images NDWI image was selected to use in class feature selection of non-water areas.

4. Results

4.1 Flood Maps as Outputs of SAR CD

Mosaicked and smoothed Sentinel-1 SAR images representing before and after flood event images for the ROI are given in Figure 6. In the VH band image, flooded areas can be seen more clearly in black color when compared to the VV band.

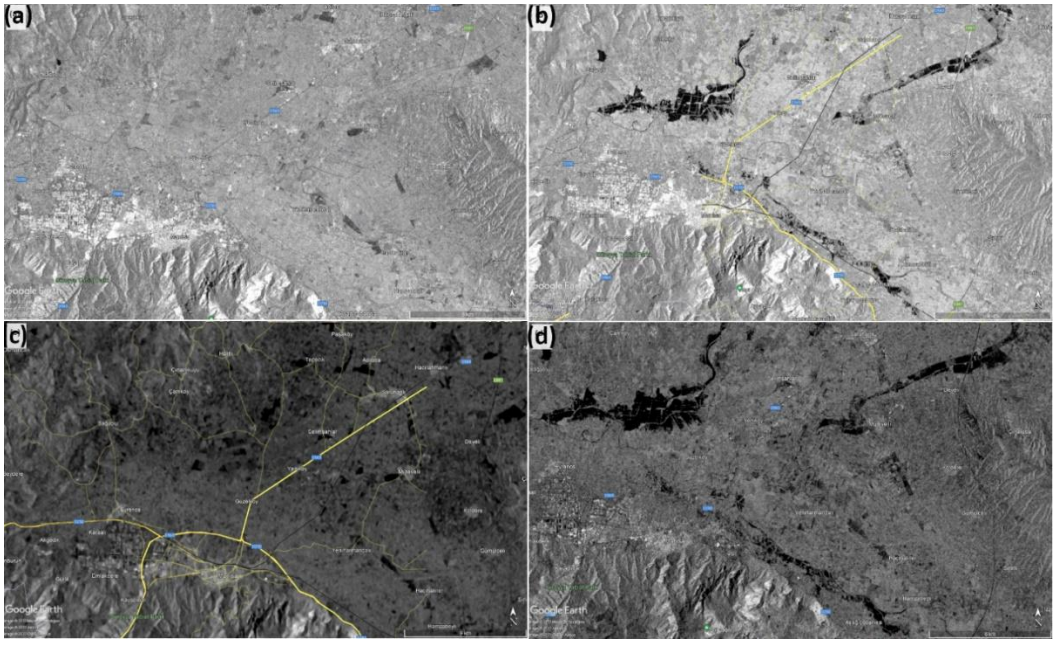

Figure 6. a) Before event VV SAR image, b) after event VV SAR image, c) before event VH image, d) after event VH image

In order to observe the changes, change detection was applied (after event minus before event) to mosaicked and smoothed SAR images for both VV and VH bands by taking their differences (Figure 7).

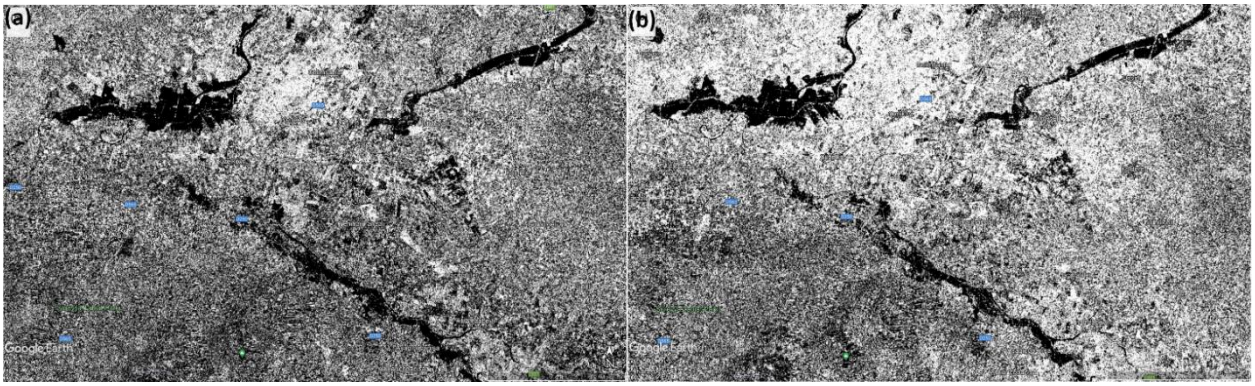

Figure 7. a) SAR difference image for VV band, b) SAR image for VH band

In Figure 7, it can be seen that the speckle effect in the image of VV band is higher than the image of VH band. The VH band image depicts the flood inundated areas more concisely.

4.2 Classification Using GEE

Mosaicked Sentinel-2 after event image was obtained from Sentinel-2 dataset with 'B2', 'B3', 'B4', 'B8', 'B11', 'B12' bands. For the training of supervised classifiers (KNN, SVM, and RF) this image was used as input with the feature collections given in Table 2 as class labels. Classified images for the three classifiers are given in Figure 8.

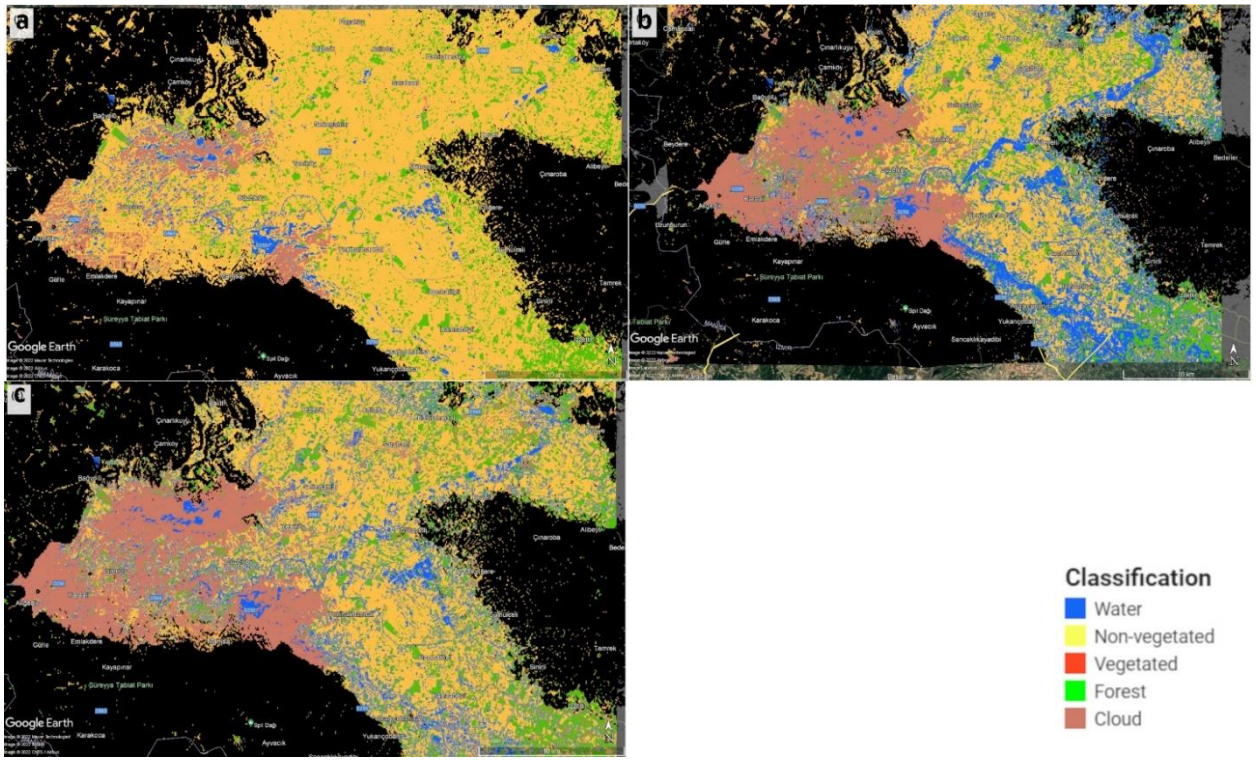

Figure 8. a) KNN classifier output, b) SVM classifier output, c) RF classifier output for Sentinel-2 MSI image composite

In Figure 8, areas classified as water can be seen in blue color. KNN classifier performs worst by depicting very small areas as clouds and water. It is a good practice to verify these results with a ground-truth image. For this purpose, inundated areas have been manually checked with the SAR difference images given in Figure 7.

It can be seen that the SVM classifier provides the most similar output to difference image in regard to the other classifiers while RF and KNN classifiers show a very speckled pattern. RF classifier shows flooded areas better than the KNN classifier but the resulting image is not satisfactory to reflect the flood inundation.

These classifiers were also applied to after flood event Sentinel-1 SAR image with the same steps applied for Sentinel-2 MSI image except for only two feature classes: water and other areas, as given in Table 2. Resulting classified outputs are given in Figure 9.

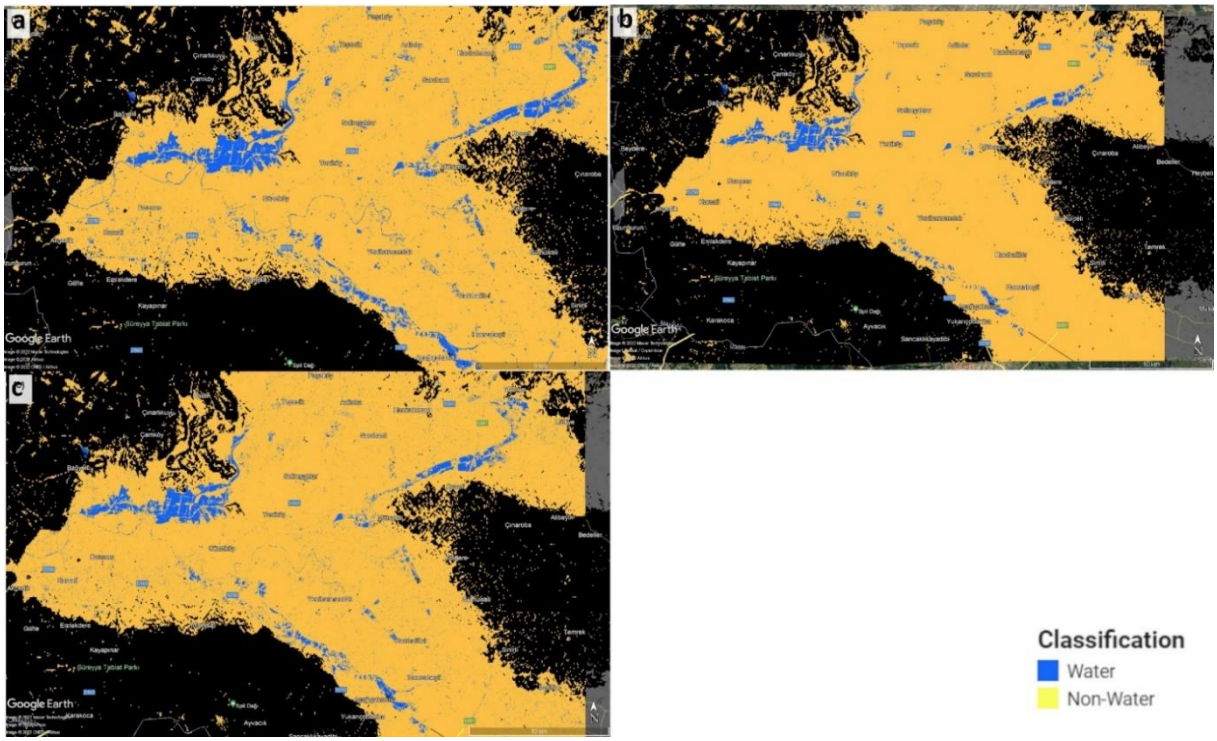

Figure 9. a) KNN classifier output, b) SVM classifier output, c) RF classifier output for Sentinel-1 SAR image

In Figure 9, areas classified as water are shown in blue color. All classifiers provide very similar outputs for flooded areas except KNN classifier predicts a wider area. When these images are checked with the SAR difference images given in Figure 7, it can be seen that flooded regions are discovered correctly by KNN classifier, but resulting in a scattered pattern.

4.3 Classification Results

Overall accuracy (OA) and Kappa coefficient values for each training/validation implementation of the three classifiers were calculated. In remote sensing, accuracy implies what proportion of the actual image was correctly predicted. The validation step was carried out to evaluate the trained model after the training processes were completed. In this step, validation data given in Table 2 was used. As said for training, validation OA was also calculated with corresponding kappa coefficient values for each classifier. Training and validation overall accuracy (OA) values of three classifiers for Sentinel-2 MSI and Sentinel-1 SAR data are given in Table 5 and Table 6, respectively.

Table 5. Training accuracy and Validation OA (%) values for Sentinel-2 MSI data

Classifier	Training	Validation	Kappa
RF	99.8	82.8	0.73
KNN	84.6	77.3	0.65
SVM	98.7	84.0	0.75

For Sentinel-2 MSI data, training accuracy values are high for both RF and SVM classifiers. SVM performs best with overall accuracy (validation) value of 84% kappa coefficient value 0.75 is substantial (>0.5) (Taati et al. 2015) as seen in

Table 5. RF classifier perform second best with OA value of 82.8% with kappa value of 0.73. KNN classifier performs worst with 77.3% OA value. Visual check comments given in Section 4.2 verify the numerical results given in Table 5.

Table 6. Training accuracy and Validation OA (%) values for Sentinel-1 SAR data

Classifier	Training	Validation	Kappa
RF	98.4	92.3	0.78
KNN	94.0	93.3	0.80
SVM	95.7	90.0	0.69

The same training and validation steps were applied to Sentinel-1 SAR after event image (VH). Differently, feature classes prepared for SAR image given in Table 2 were used for sampling. Two classes were enough to represent the image as water and other areas. When the OA results given in Table 6 are considered, it is obvious that, training and validation values are high for RF, KNN and SVM classifiers where all kappa values show good agreement (<=0.8). These results reflect the classifier outputs given in Figure 9 where KNN classifier provides the highest validation and kappa values, consistent with manual image interpretations.

5. Discussion and Conclusion

In this study, flood inundation mapping of an extensive part of the Gediz plain for a flood event that occurred on 02.02.2021 was presented. European Space Agency (ESA) provides Sentinel-1 SAR and Sentinel-2 multispectral images free of charge. Google Earth Engine (GEE) presents a free cloud service for high-performance computing in a bundle of Machine Learning (ML) algorithms and a large amount of satellite data for public use. We have taken advantage of cloud computing via GEE to map inundated areas in Gediz plain by examining the SAR images in a traditional change detection approach. Supervised classification was performed by using the built-in GEE ML algorithms: RF, KNN, and SVM.

SAR change detection images were used for validation of the supervised classification results because of the lack of ground truth for the study area on the event day. Results imply a major point in image classification with supervised classifiers. The point is the selection of the polygons for training and validation. RF and SVM gives very high training accuracy values as 99.8% and 98.7%, respectively. A large polygon set was composed for training in the study and these high values imply the sufficiency of this dataset. Also overfitting can be seen for SVM and RF classifiers in the lower right part of Figure 8.b when compared with the corresponding Sentinel-1 SAR imagery. When this region was investigated it has been observed that there does not exist any train and validation polygons in the right lower bound of the study area. This was done intentionally because the blue pixels in SWIR composite (Figure 2) regarding this region was not absolutely blue, conversely these regions were heterogeneous with a combination with some white, black, blue pixels. It would increase noise if these regions were labelled. This claim also supports the best OA values of RF and SVM classifiers. SVM performs best with overall accuracy value of 84% kappa coefficient value 0.75. SVM is advantageous in image classification problems where input/output dependencies are unknown. Regarding the noisy nature of the training dataset robustness of SVM classifier gives the best OA values among other classifiers.

Same classifiers were applied to Sentinel-1 SAR after event image with unique training and validation polygons. The best performing classifier for SAR image was KNN classifier with an OA value of 93.3% and a good kappa value 0.80. RF classifier performs very near to KNN classifier with an OA value of 92.3% and a good kappa value 0.78. This classification was implemented with two classes and noise in data is very low because of two pixel values: black or white. Although KNN and RF classifiers give near OA values, KNN classifier output is very similar to SAR difference images in Figure 7. RF classifier output should be very near to this result, the cause could be overfitting with a 98.4% training accuracy value.

During and after the heavy rainfall, Sentinel-2 MSI images were covered with clouds. Even though, after the event image cloud rate was low in rate, cloudy regions in the image affected the classifiers in a negative way by covering a large extent of the flooded area. Classifiers were trained with Sentinel-1 SAR and Sentinel-2 MSI images to acquire the best result. The best accuracy results were acquired by the SVM classifier for the optical and kNN classifier for the SAR after event images. It was hard challenging to hand label polygons in Sentinel-2 MSI images. To improve the results a large number of polygons were labelled. Results of the study verify the efficiency of SAR images in all-weather and their robustness to clouds.

Acknowledgement

This study is supported by Çukurova University Scientific Research Projects Coordination Unit under grant number: FBA-2021-14022.

References

Afify, H. A. (2011). Evaluation of change detection techniques for monitoring land-cover changes: A case study in new Burg El-Arab area. *Alexandria Engineering Journal*, *50*(2), 187-195.

Amani, M., Brisco, B., Afshar, M., Mirmazloumi, S. M., Mahdavi, S., Mirzadeh, S. M. J., & Granger, J. (2019). A generalized supervised classification scheme to produce provincial wetland inventory maps: An application of Google Earth Engine for big geo data processing. *Big Earth Data*, *3*(4), 378-394.

Arslan, D., Çiçek, K., Döndüren, Ö., & Ernoul, L. (2021). Threat ranking to improve conservation planning: an example from the Gediz Delta, Turkey. *Land*, *10*(12), 1381. doi: 10.3390/land10121381.

Baghi, A., & Karami, A. (2017). SAR image segmentation using region growing and spectral cluster. In *3rd International Conference on Pattern Recognition and Image Analysis (IPRIA), 2017. Proceedings.* (pp. 229-232). IEEE.

Benoudjit, A., & Guida, R. (2019). A novel fully automated mapping of the flood extent on SAR images using a supervised classifier. *Remote Sensing, 11*(7), 779. doi: 10.3390/rs11070779.

Breiman, L. (2001). Random forests. *Machine Learning, 45*(1), 5-32.

Brown, K. M., Hambidge, C. H., & Brownett, J. M. (2016). Progress in operational flood mapping using satellite synthetic aperture radar (SAR) and airborne light detection and ranging (LiDAR) data. *Progress in Physical Geography, 40*(2), 196-214.

Cao, H., Zhang, H., Wang, C., & Zhang, B. (2019). Operational flood detection using Sentinel-1 SAR data over large areas. *Water, 11*(4), 786. doi: 10.3390/w11040786.

Carincotte, C., Derrode, S., & Bourennane, S. (2006). Unsupervised change detection on SAR images using fuzzy hidden Markov chains. *IEEE Transactions on Geoscience and Remote Sensing, 44*(2), 432-441.

Chang, Y. L., Anagaw, A., Chang, L., Wang, Y. C., Hsiao, C. Y., & Lee, W. H. (2019). Ship detection based on YOLOv2 for SAR imagery. *Remote Sensing, 11*(7), 786. doi: 10.3390/rs11070786.

Chen, Y., Li, J., & Chen, A. (2021). Does high risk mean high loss: Evidence from flood disaster in southern China. *Science of The Total Environment*, *785*, 147127. doi: 10.1016/j.scitotenv.2021.147127.

Cian, F., Marconcini, M., Ceccato, P., & Giupponi, C. (2018). Flood depth estimation by means of high-resolution SAR images and lidar data. *Natural Hazards and Earth System Sciences, 18*(11), 3063-3084.

Clement, M. A., Kilsby, C. G., & Moore, P. (2018). Multi-temporal synthetic aperture radar flood mapping using change detection. *Journal of Flood Risk Management, 11*(2), 152-168.

Cohen, J. (1960). A coefficient of agreement for nominal scales. *Educational and Psychological Measurement*, *20*(1), 37-46.

Čotar, K., Oštir, K., & Kokalj, Ž. (2016). Radar satellite imagery and automatic detection of water bodies. *Geodetski glasnik*, *50*(47), 5-15.

ÇOB. (2007). *Gediz Deltası Sulak Alan Yönetim Planı*. Ankara: T.C. Çevre ve Orman Bakanlığı, Doğa Koruma ve Milli Parklar, Sulak Alanlar Şube Müdürlüğü.

Damtea, W., Kim, D., & Im, S. (2020). Spatiotemporal analysis of land cover changes in the chemoga basin, Ethiopia, using Landsat and google earth images. *Sustainability*, *12*(9), 3607. doi: 10.3390/su12093607.

Duda, R. O., Hart, P. E., & Stork, D. G. (1973). *Pattern classification and scene analysis*. New York, NY: Wiley.

Goffi, A., Stroppiana, D., Brivio, P. A., Bordogna, G., & Boschetti, M. (2020). Towards an automated approach to map flooded areas from Sentinel-2 MSI data and soft integration of water spectral features. *International Journal of Applied Earth Observation and Geoinformation*, *84*, 101951. doi:10.1016/j.jag.2019.101951.

Gorelick, N., Hancher, M., Dixon, M., Ilyushchenko, S., Thau, D., & Moore, R. (2017). Google Earth Engine: Planetary-scale geospatial analysis for everyone. *Remote sensing of Environment*, *202*, 18-27.

Hardisky, M.A., Klemas, V., & Smart, R. (1983). The influence of soil salinity, growth form, and leaf moisture on-the spectral radiance of Spartina alterniflora Canopies. *Photogrammetric Engineering and Remote Sensing, 49*(1), 77-83.

Hsu, C.-W., Chang, C.-C., & Lin, C.-J. (2016). *A practical guide to support vector classification*. Retrieved from https://www.csie.ntu.edu.tw/~cjlin/papers/guide/guide.pdf.

Klemas, V. (2013). Remote sensing of emergent and submerged wetlands: An overview. *International Journal of Remote Sensing*, *34*(18), 6286-6320.

Kurita, T., Otsu, N., & Abdelmalek, N. (1992). Maximum likelihood thresholding based on population mixture models. *Pattern Recognition, 25*(10), 1231-1240.

Martinis, S., Kuenzer, C., Wendleder, A., Huth, J., Twele, A., Roth, A., & Dech, S. (2015). Comparing four operational SAR-based water and flood detection approaches. *International Journal of Remote Sensing*, *36*(13), 3519-3543.

McFeeters, S. K. (1996). The use of the Normalized Difference Water Index (NDWI) in the delineation of open water features. *International Journal of Remote Sensing*, *17*(7), 1425-1432.

MGM, (2023). *Resmi İstatistikler, İllere Ait Mevsim Normalleri (1991-2020)*. Retrieved from https://mgm.gov.tr/veridegerlendirme/il-ve-ilceler-istatistik.aspx?k=H&m=MANISA.

Ozkan, S. P., & Tarhan, C. (2016). Detection of flood hazard in urban areas using GIS: Izmir case. *Procedia Technology*, *22*, 373-381.

Pradhan, B., Hagemann, U., Tehrany, M. S., & Prechtel, N. (2014). An easy to use ArcMap based texture analysis program for extraction of flooded areas from TerraSAR-X satellite image. *Computers & Geosciences*, *63*, 34-43.

Pramanick, N., Acharyya, R., Mukherjee, S., Mukherjee, S., Pal, I., Mitra, D. & Mukhopadhyay, A. (2022). SAR based flood risk analysis: A case study Kerala flood 2018. *Advances in Space Research*, *69*(4), 1915-1929.

Rouse, J. W., Haas, R. H., Schell, J. A., & Deering, D. W. (1974). Monitoring vegetation systems in the Great Plains with ERTS. In *Third Earth Resources Technology Satellite-1 Symposium, 1974. Proceedings*. (pp. 309-317). NASA.

Schumann, G., Di Baldassarre, G., Alsdorf, D., & Bates, P. D. (2010). Near real-time flood wave approximation on large rivers from space: Application to the River Po, Italy. *Water Resources Research*, *46*(5), W05601. doi: 0.1029/2008WR007672.

Solbø, S., & Solheim, I. (2005, September). Towards operational flood mapping with satellite SAR. In *Envisat & ERS Symposium, 2004. Proceedings.* (pp. 1-8).

Taati, A., Sarmadian, F., Mousavi, A., Pour, C. T. H., & Shahir, A. H. E. (2015). Land use classification using support vector machine and maximum likelihood algorithms by Landsat 5 TM images. *Walailak Journal of Science and Technology (WJST), 12*(8), 681-687.

Taheri Dehkordi, A., Valadan Zoej, M. J., Ghasemi, H., Ghaderpour, E., & Hassan, Q. K. (2022). A new clustering method to generate training samples for supervised monitoring of long-term water surface dynamics using Landsat data through Google Earth Engine. *Sustainability*, *14*(13), 8046. doi: 10.3390/su14138046.

Thanh Noi, P., & Kappas, M. (2017). Comparison of random forest, k-nearest neighbor, and support vector machine classifiers for land cover classification using Sentinel-2 imagery. *Sensors*, *18*(1), 18. doi: 10.3390/s18010018.

Topouzelis, K. N. (2008). Oil spill detection by SAR images: dark formation detection, feature extraction and classification algorithms. *Sensors*, *8*(10), 6642-6659.

Xu, H. (2006). Modification of normalised difference water index (NDWI) to enhance open water features in remotely sensed imagery. *International Journal of Remote Sensing*, *27*(14), 3025-3033.